Chapter 6 Core-Collapse Supernova Neutrinos

Neutrinos emitted in the first few seconds of a core-collapse supernova carry with them the potential for great insight into the mechanisms behind some of the most spectacular events that have played key roles in the evolution of the Universe. Collection and analysis of this high-statistics neutrino signal from a supernova within our galaxy would provide a rare opportunity to witness the energy and flavor development of the burst as a function of time. This would in turn shed light on the astrophysics of the collapse as well as on neutrino properties.

6.1 The Neutrino Signal and Astrophysical Phenomena

A core-collapse supernova* occurs when a massive star reaches the end of its life, and stellar burning can no longer support the star's weight. This catastrophic collapse results in a compact remnant such as a neutron star, or possibly a black hole, depending on the mass of the progenitor. The infall is followed by a *bounce* when sufficiently high core density is reached, and in some unknown (but nonzero) fraction of cases, the shock wave formed after the bounce results in a bright explosion [1]. The explosion energy represents only a small fraction of the enormous total gravitational binding energy of the resulting compact remnant, however — thanks to the neutrinos' weak coupling, which allows them to escape — within a few tens of seconds almost all of the energy is emitted in the form of neutrinos in the tens-of-MeV range. In spite of their weak coupling, the neutrinos are copious enough to (very likely) play a significant role in the explosion.

Neutrinos from the celebrated SN1987A core collapse [2,3] in the Large Magellanic Cloud outside the Milky Way were observed; however, the statistics were sparse and a great many questions remain. A high-statistics observation of a neutrino burst from a nearby supernova would be possible with the current generation of detectors. Such an observation would shed light on the nature of the astrophysical event, as well as on the nature of neutrinos themselves. Sensitivity to the different flavor components of the flux is highly desirable.

The core-collapse neutrino signal starts with a short, sharp *neutronization* burst primarily composed of ν_e (originating from $p + e^- \rightarrow n + \nu_e$, as protons and electrons get squeezed together), and is followed by an *accretion* phase lasting some hundreds of milliseconds, as matter falls onto the collapsed core. The later *cooling* phase over $\sim$10 seconds represents the main part of the signal, over which the proto-neutron star sheds its gravitational binding energy. The neutrino flavor con-

Supernova always refers to a *core-collapse supernova* in this chapter unless stated otherwise.

tent and spectra change throughout these phases, and the supernova's temperature evolution can be followed with the neutrino signal. Some fairly generic supernova signal features are illustrated in Figure 6.1, based on [4] and reproduced from [5].

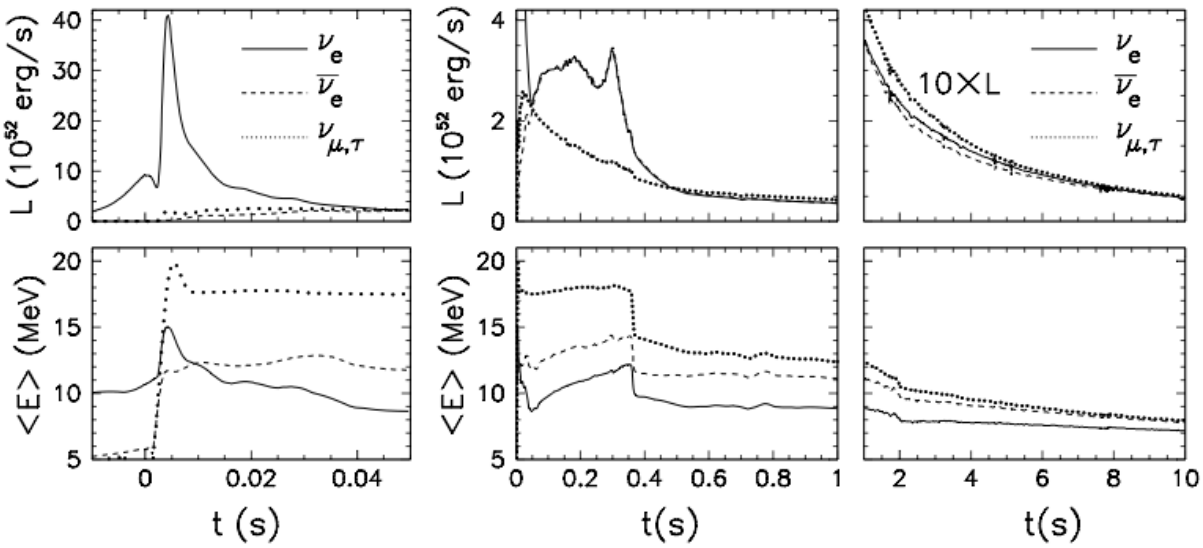

Figure 6.1: Expected core-collapse neutrino signal from the *Basel* model [4], for a 10.8 $M_\odot$ progenitor. The left plots show the very early signal, including the neutronization burst; the middle plots show the accretion phase, and the right plots show the cooling phase. Luminosities as a function of time are shown across the top plots. The bottom plots show average energy as a function of time for the ν_e, $\overline{\nu}_e$ and $\nu_{\mu,\tau}$ flavor components of the flux (fluxes for ν_μ, $\overline{\nu}_\mu$, ν_τ, and $\overline{\nu}_\tau$ should be identical). Figure courtesy of [5].

The supernova-neutrino spectrum at a given moment in time is expected to be well described by a parameterization [6,7] given by:

$$\phi(E_\nu) = \mathcal{N}\left(\frac{E_\nu}{\langle E_\nu\rangle}\right)^{\alpha} \exp\left[-\left(\alpha+1\right)\frac{E_\nu}{\langle E_\nu\rangle}\right] , \tag{6.1}$$

where E_ν is the neutrino energy, $\langle E_\nu\rangle$ is the mean neutrino energy, α is a *pinching parameter*, and $\mathcal{N}$ is a normalization constant. Large α corresponds to a more pinched spectrum (suppressed high-energy tail). This parameterization is referred to as a *pinched-thermal* form. The different ν_e, $\overline{\nu}_e$ and ν_x, $x = \mu, \tau$ flavors are expected to have different average energy and α parameters and to evolve differently in time.

A wide variety of astrophysical phenomena affect the flavor-energy-time evolution of the spectrum, including neutrino oscillation effects that are determined by the mass hierarchy (MH) and *collective* effects due to neutrino-neutrino interactions. A voluminous literature exists exploring these collective phenomena, e.g., [8,9,10,11,12,13,14,15,16].

A number of astrophysical phenomena associated with supernovae are expected to be observable in the supernova-neutrino signal, providing a remarkable window into the event, for example:

- The initial burst, primarily composed of ν_e and called the *neutronization* or *breakout* burst, represents only a small component of the total signal. However, oscillation effects can manifest in an observable manner in this burst, and flavor transformations can be modified by the *halo* of neutrinos generated in the supernova envelope by scattering [17].
- The formation of a black hole would cause a sharp signal cutoff (e.g., [18,19]).
- Shock wave effects (e.g., [20]) would cause a time-dependent change in flavor and spectral composition as the shock wave propagates.
- The standing accretion shock instability (SASI) [21,22], a *sloshing* mode predicted by 3D neutrino-hydrodynamics simulations of supernova cores, would give an oscillatory flavor-dependent modulation of the flux.
- Turbulence effects [23,24] would also cause flavor-dependent spectral modification as a function of time.

This list is far from comprehensive. Furthermore, signatures of *collective* effects and signatures that depend on the MH will make an impact on many of the above signals (examples will be presented in Section 6.2). Certain phenomena are even postulated to indicate beyond-the-Standard-Model physics [25] such as axions, extra dimensions and an anomalous neutrino magnetic moment; non-observation of these effects, conversely, would enable constraints on these phenomena.

The supernova-neutrino burst signal is prompt with respect to the electromagnetic signal and therefore can be exploited to provide an early warning to astronomers [26,27]. Additionally, a LArTPC signal [28] is expected to provide some pointing information, primarily from elastic scattering on electrons.

Even non-observation of a burst, or non-observation of a ν_e component of a burst in the presence of supernovae (or other astrophysical events) observed in electromagnetic or gravitational wave channels, would still provide valuable information about the nature of the sources. Moreover, a long-timescale, sensitive search yielding no bursts will also provide limits on the rate of core-collapse supernovae.

6.2 Expected Signal and Detection in Liquid Argon

As discussed in Section 2.4, liquid argon is known to exhibit a singular sensitivity to the ν_e component of a supernova-neutrino burst. This feature is especially important, as it will make LBNE a unique source in the global effort to combine data from a variety of detectors with different flavor sensitivities to obtain a complete picture of the physics of the burst.

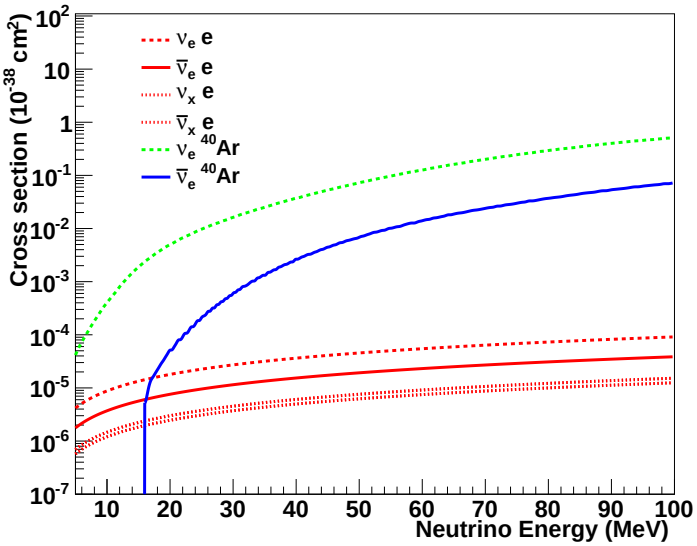

Figure 6.2: Cross sections for supernova-relevant interactions in argon.

The predicted event rate from a supernova-neutrino burst may be calculated by folding expected neutrino differential energy spectra in with cross sections for the relevant channels, and with detector response. For event rate estimates in liquid argon, a detection threshold of 5 MeV is assumed. The photon-detection system of the LBNE far detector, coupled with charge collection and simple pattern recognition, is expected to provide a highly efficient trigger. Most LBNE supernova physics sensitivity studies so far have been done using parameterized detector responses from [29] implemented in the SNOwGLoBES software package [30]. SNOwGLoBES takes as input fluxes, cross sections (Figure 6.2), *smearing matrices* (that incorporate both interaction product spectra and detector response) and post-smearing efficiencies. The energy resolution used is

$$\frac{\sigma}{E\ (\mathrm{MeV})} = \frac{11\%}{\sqrt{E\ \mathrm{MeV}}} + 2\% \tag{6.2}$$

Work is currently underway using the full Geant4 simulation [31] framework and the LArSoft software package [32] to characterize low-energy response for realistic LBNE detector configurations. Preliminary studies of the detector response with the full simulation are summarized in Section A.1.2 and are found to be consistent with the parameterized response implemented in SNOwGLoBES.

Table 6.1 shows rates calculated with SNOwGLoBES for the dominant interactions in argon for the *Livermore* model [33], and the *GKVM* model [34]. Figure 6.3 shows the expected observed differential event spectra for these fluxes. Clearly, the ν_e flavor dominates.

Table 6.1: Event rates for different supernova models in 34 kt of liquid argon for a core collapse at 10 kpc, for ν_e and $\overline{\nu}_e$ charged-current channels and elastic scattering (ES) on electrons. Event rates will simply scale by active detector mass and inverse square of supernova distance.

Channel	Events *Livermore* model	Events *GKVM* model
$\nu_e + {}^{40}\mathrm{Ar} \rightarrow e^- + {}^{40}\mathrm{K}^*$	2308	2848
$\overline{\nu}_e + {}^{40}\mathrm{Ar} \rightarrow e^+ + {}^{40}\mathrm{Cl}^*$	194	134
$\nu_x + e^- \rightarrow \nu_x + e^-$	296	178
Total	**2794**	**3160**

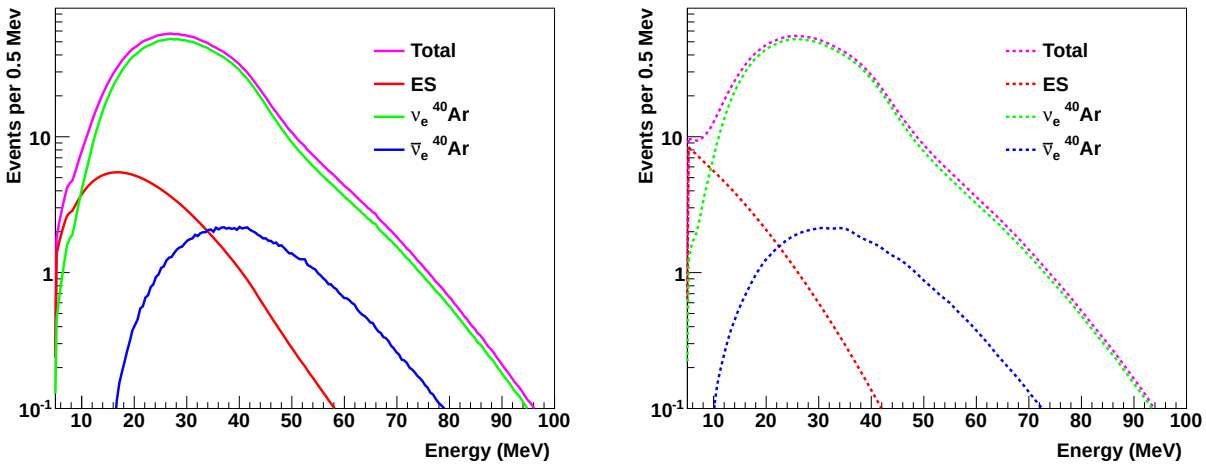

Figure 6.3: Supernova-neutrino event rates in 34 kt of argon for a core collapse at 10 kpc, for the GKVM model [34] (events per 0.5 MeV), showing three relevant interaction channels. Left: interaction rates as a function of true neutrino energy. Right: *smeared* rates as a function of detected energy, assuming resolution from [29].

Figure 6.4 gives another example of an expected burst signal, for which a calculation with detailed time dependence of the spectra is available [35] out to nine seconds post-bounce. This model has relatively low luminosity but a robust neutronization burst. Note that the relative fraction of neutronization-burst events is quite high.

In Figure 6.5, different oscillation hypotheses have been applied to *Duan* fluxes [16]. The Duan flux represents only a single late time slice of the supernova-neutrino burst and not the full flux; MH information will be encoded in the time evolution of the signal, as well. The figure illustrates, if only anecdotally, potential MH signatures.

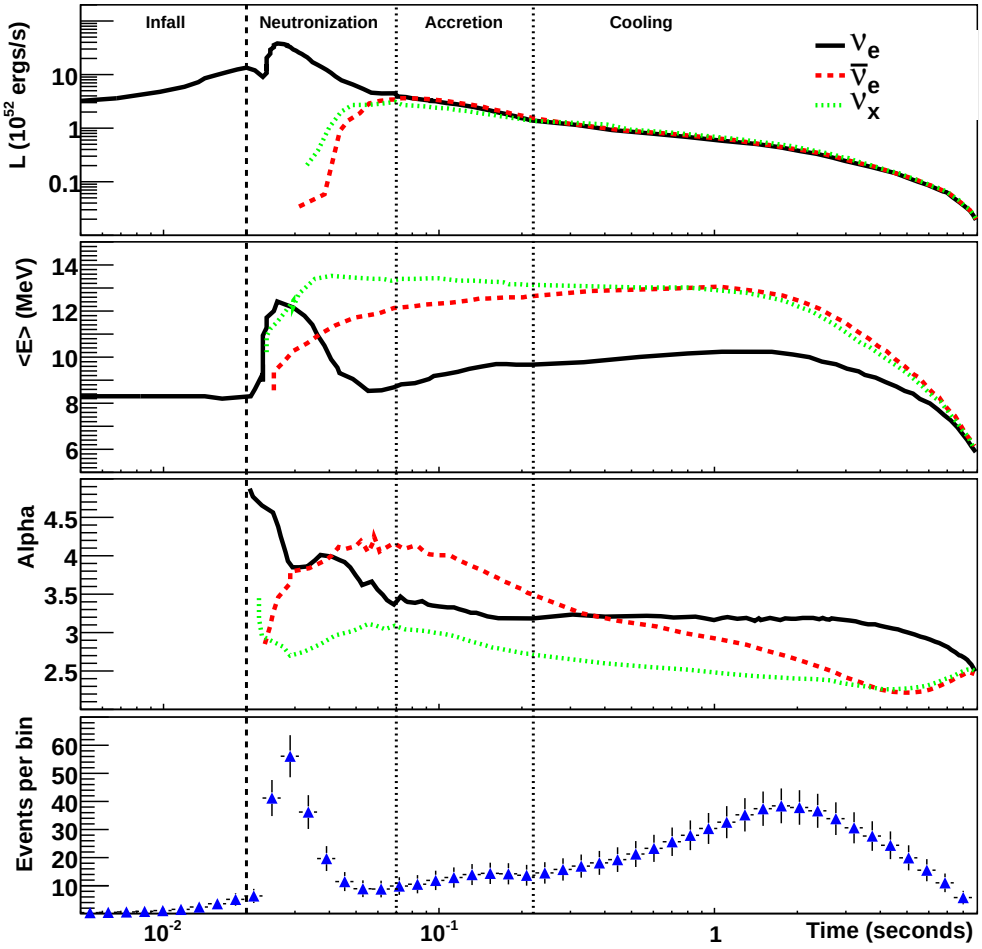

Figure 6.4: Expected time-dependent signal for a specific flux model for an electron-capture supernova [35] at 10 kpc. The top plot shows the luminosity, the second plot shows average neutrino energy, and the third plot shows the α (pinching) parameter. The fourth (bottom) plot shows the total number of events (mostly ν_e) expected in 34 kt of liquid argon, calculated using SNoWGLoBES. Note the logarithmic binning in time; the plot shows the number of events expected in the given bin and the error bars are statistical. The vertical dashed line at 0.02 seconds indicates the time of core bounce, and the vertical lines indicate different eras in the supernova evolution. The leftmost time interval indicates the infall period. The next interval, from core bounce to 50 ms, is the neutronization burst era, in which the flux is composed primarily of ν_e. The next period, from 50 to 200 ms, is the accretion period. The final era, from 0.2 to 9 seconds, is the proto-neutron-star cooling period.

Another potential MH signature is shown in Figure 6.6, for which a clear time-dependent shock-wave-related feature is visible for the normal MH case.

Figure 6.7 shows yet another example of a preliminary study showing how one might track supernova temperature as a function of time with the ν_e signal in liquid argon. Here, a fit is made to the pinched-thermal form of Equation 6.1. Not only can the internal temperature of the supernova be effectively measured, but the time evolution is observably different for the different hierarchies.

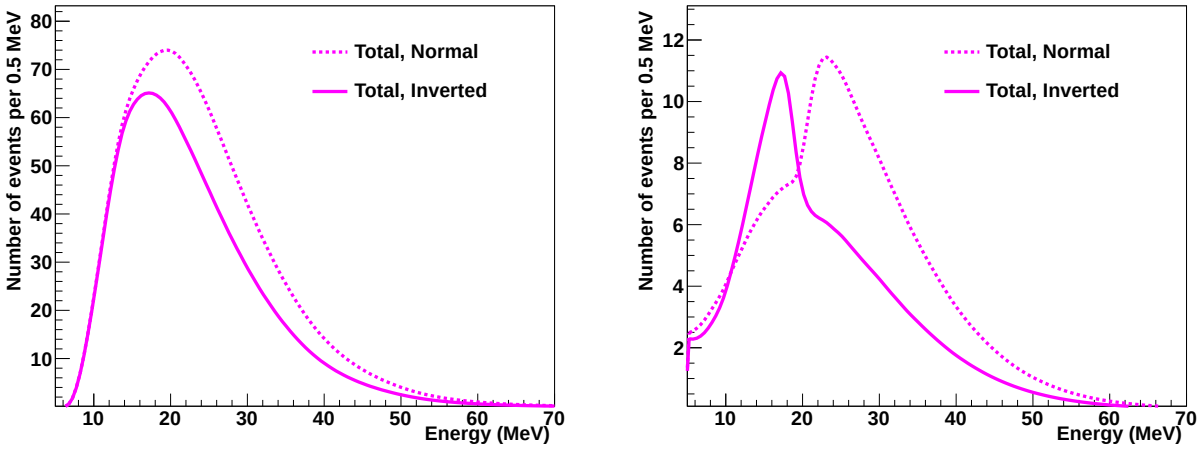

Figure 6.5: Comparison of total event rates for normal and inverted MH, for a specific flux example, for a 100-kt water Cherenkov detector (left) and for a 34-kt LArTPC (right) configuration, in events per 0.5 MeV. There are distinctive features in liquid argon for different neutrino mass hierarchies for this supernova model [36].

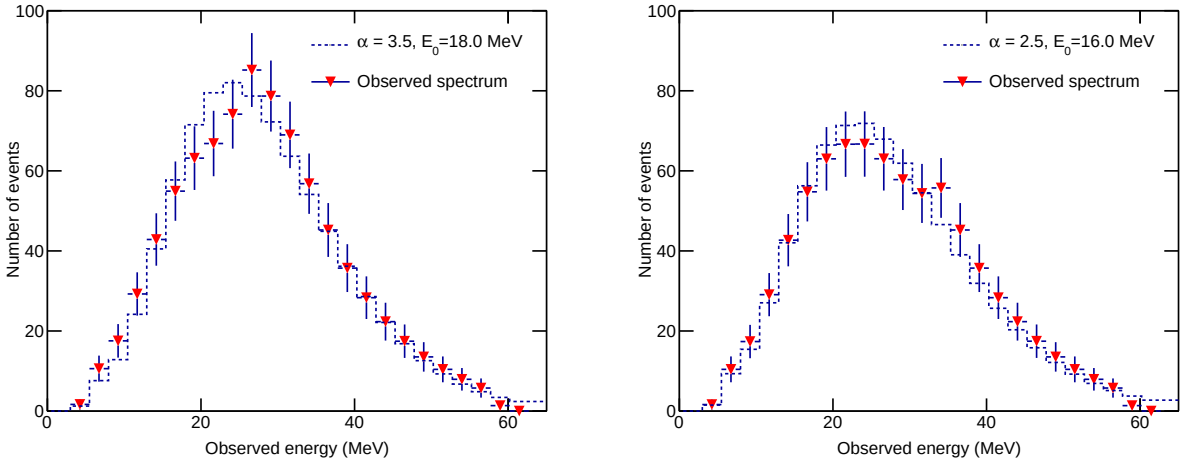

Figure 6.6: Observed ν_e spectra in 34 kt of liquid argon for a 10-kpc core collapse, representing about one second of integration time each at one-second intervals during the supernova cooling phase. The dashed line represents the best fit to a parameterized pinched-thermal spectrum. Clear *non-thermal* features in the spectrum that change with time are visible, on the left at around 20 MeV and on the right at around 35 MeV. Error bars are statistical. These features are present *only* for the normal MH.

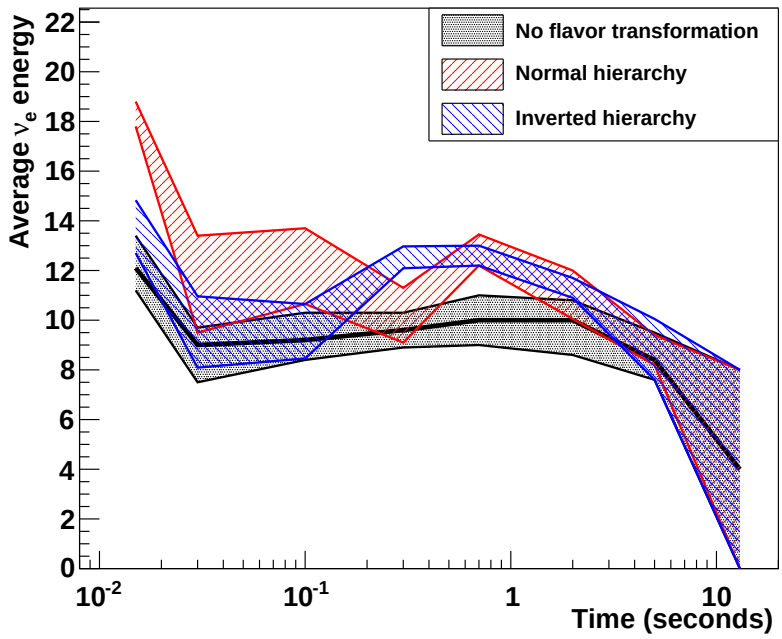

Figure 6.7: Average ν_e energy from fit to SNOwGLoBES-smeared, pinched-thermal spectrum as a function of time (34 kt at 10 kpc), for a flux model based on [37] and including collective oscillations, for two different MH assumptions. The bands represent 1σ error bars from the fit. The solid black line is the truth $\langle E_\nu \rangle$ for the unoscillated spectrum. Clearly, meaningful information can be gleaned by tracking ν_e spectra as a function of time.

6.3 Low-Energy Backgrounds

6.3.1 Cosmic Rays

Due to their low energy, supernova-neutrino events are subject to background from cosmic rays, although the nature of the signal — a short-timescale burst — is such that the background from these muons and their associated Michel electrons can in principle be well known, easily distinguished and subtracted. Preliminary studies [38] suggest that the shielding provided by the 4,850-ft depth available at the Sanford Underground Research Facility is acceptable.

6.3.2 Local Radiation Sources

It is possible that radioactive decays will directly overlap with the energy spectrum created by supernova-neutrino events in LBNE. It is also possible for an ensemble of radioactive-decay events in and around higher-energy particle interactions (e.g., from beam neutrinos) to obscure the edges of electromagnetic showers from highly scattering particles such as electrons and pions; this would appear as the radiological equivalent of dark noise in a digital image, and could potentially intro-

duce a systematic uncertainty in the energy calculated for events, even at much higher energy than the decays themselves. It is therefore very important to calculate the radioactive-decay backgrounds in the LBNE far detector with sufficient accuracy to properly account for their presence, either as direct backgrounds or as systematic effects in energy calculations. To this end, LBNE collaborators are in the process of creating a physics-driven, radioactive-background budget and associated event generator for low-energy background events in the far detector.

The radioactive-background budget will have many components, each of which will fall into one of two categories:

1. intrinsic radioactive contamination in the argon or support materials, or
2. cosmogenic radioactivity produced in situ from cosmic-ray showers interacting with the argon or the support materials.

The former is dependent on the detector materials, and is therefore independent of far detector depth. The latter is strongly coupled to the cosmic-ray flux and spectrum. A preliminary estimate [39] of the cosmogenic radioactivity from beta emitters produced from cosmic-ray interactions with argon in the LBNE far detector at the 4,850 ft level of the Sanford Underground Research Facility is shown in Figure 6.8. Both of these background categories add to the direct energy depositions from cosmic rays themselves and associated showers.

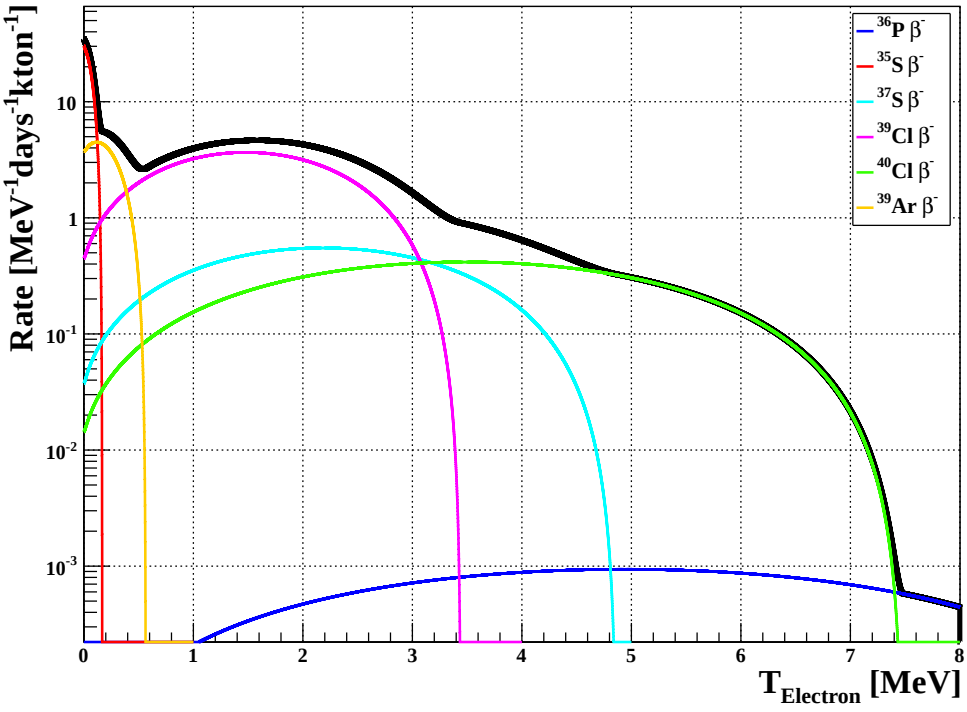

Figure 6.8: Cosmogenic background rates in the LBNE LArTPC as a function of the decay beta kinetic energy calculated at the 4,850-ft level of the Sanford Underground Research Facility.

6.3.3 Intrinsic Radioactive Background Mitigation

Intrinsic backgrounds in the far detector come from the radioactive material that is prevalent in the detector materials (both active and instrumentation/support materials and the cryostat itself), in the cavern walls and in the dust [40]. The isotopes of primary interest are "the usual suspects" in experiments where radioactive backgrounds must be controlled: ^{232}Th and ^{238}U (and their associated decay chains), ^{40}K, and ^{60}Co. In addition, ^{39}Ar will contribute a significant component, since it is present in natural argon harvested from the atmosphere at the level of approximately 1 Bq/kg. In consequence, a 10-kt far detector filled with $^{\mathrm{nat.}}$Ar will experience a rate from ^{39}Ar of approximately 10 MHz across the whole detector. The beta decay spectrum from ^{39}Ar is thankfully quite low in energy (Q_β = 0.565 MeV), so it will not interfere directly with the supernova signal, but it may contribute to the *dark noise* effect. Furthermore, the product of the average beta energy with this rate indicates the level at which the background due to introduction of power into the detector becomes a problem. This radioactive power from ^{39}Ar is approximately:

$$P_{Rad} \sim 0.25 \text{ MeV} \times 10 \text{ MHz} = 2.5 \times 10^6 \text{ MeV/s}. \tag{6.3}$$

Because this category of background can come from the cavern walls, the concrete cavern lining, the cryostat materials or the materials that compose the submersed instrumentation, it is important to know which type of radioactive decay is produced by each isotope as well as the total energy it releases. For instance, an alpha decay from an isotope in the U or Th decay chain will deposit its full energy into the detector if it occurs in the active region of the detector, but will deposit no energy if it occurs inside of some macroscopically thick piece of support material because of its very short range ($\lesssim$1 μm) in most solids. This requires different accounting for energy depositions from intrinsic radioactive contamination measured in different locations (or groups of locations). This is clearly a tractable problem, but one which must be handled with care and forethought.

Since a large body of work has been compiled on the control of radiological background in previous experiments that have encountered similar conditions, much of the work in this area will be cited from these experiments (e.g., DARKSIDE [41], EXO [42], ICARUS, BOREXINO, KamLAND and Super–Kamiokande). Work remains, however, on understanding the background particular to the LBNE far detector location/depth (e.g., radon levels and dust activity, for instance), and on integrating existing and new work into the LBNE simulation, reconstruction and analysis framework.

6.4 Summary of Core-Collapse Supernova Sensitivities

LBNE, with its high-resolution LArTPC far detector, is uniquely sensitive to the ν_e component of the neutrino flux from a core-collapse supernova within our galaxy. The ν_e component of the neutrino flux dominates the initial neutronization burst of the supernova. Preliminary studies indicate that such a supernova at a distance of 10 kpc would produce $\sim$3,000 events in a 34-kt LArTPC. The time dependence of the signal will allow differentiation between different neutrino-driven core-collapse dynamical models, and will exhibit a discernible dependence on the neutrino mass hierarchy.

A low energy threshold of $\sim$ 5 MeV will enable the detector to extract the rich information available from the ν_e supernova flux. LBNE's photon detection system is being designed to provide a high-efficiency trigger for supernova events. Careful design and quality control of the detector materials will minimize low-energy background from radiological contaminants.

References

1. H.-T. Janka, "Explosion Mechanisms of Core-Collapse Supernovae," *Ann.Rev.Nucl.Part.Sci.* **62** (2012) 407–451, arXiv:1206.2503 [astro-ph.SR]. Cited in Section 6.1 (pg.151).
2. R. Bionta, G. Blewitt, C. Bratton, D. Casper, A. Ciocio, *et al.*, "Observation of a Neutrino Burst in Coincidence with Supernova SN 1987a in the Large Magellanic Cloud," *Phys.Rev.Lett.* **58** (1987) 1494. Cited in Section 6.1 (pg.151).
3. K. Hirata *et al.*, **KAMIOKANDE-II Collaboration** , "Observation of a Neutrino Burst from the Supernova SN 1987a," *Phys.Rev.Lett.* **58** (1987) 1490–1493. Cited in Section 6.1 (pg.151).
4. T. Fischer, S. Whitehouse, A. Mezzacappa, F.-K. Thielemann, and M. Liebendorfer, "Protoneutron star evolution and the neutrino driven wind in general relativistic neutrino radiation hydrodynamics simulations," *Astron.Astrophys.* **517** (2010) A80, arXiv:0908.1871 [astro-ph.HE]. Cited in Section 6.1 (pg.152).
5. M. Wurm *et al.*, **LENA Collaboration** , "The next-generation liquid-scintillator neutrino observatory LENA," *Astropart.Phys.* **35** (2012) 685–732, arXiv:1104.5620 [astro-ph.IM]. Cited in Section 6.1 (pg.152).
6. H. Minakata, H. Nunokawa, R. Tomas, and J. W. Valle, "Parameter Degeneracy in Flavor-Dependent Reconstruction of Supernova Neutrino Fluxes," *JCAP* **0812** (2008) 006, arXiv:0802.1489 [hep-ph]. Cited in Section 6.1 (pg.152).
7. I. Tamborra, B. Muller, L. Hudepohl, H.-T. Janka, and G. Raffelt, "High-resolution supernova neutrino spectra represented by a simple fit," *Phys.Rev.* **D86** (2012) 125031, arXiv:1211.3920 [astro-ph.SR]. Cited in Section 6.1 (pg.152).
8. H. Duan, G. M. Fuller, and Y.-Z. Qian, "Collective neutrino flavor transformation in supernovae," *Phys.Rev.* **D74** (2006) 123004, arXiv:astro-ph/0511275 [astro-ph]. Cited in Section 6.1 (pg.152).
9. G. L. Fogli, E. Lisi, A. Marrone, and A. Mirizzi, "Collective neutrino flavor transitions in supernovae and the role of trajectory averaging," *JCAP* **0712** (2007) 010, arXiv:0707.1998 [hep-ph]. Cited in Section 6.1 (pg.152).
10. G. G. Raffelt and A. Y. Smirnov, "Self-induced spectral splits in supernova neutrino fluxes," *Phys.Rev.* **D76** (2007) 081301, arXiv:0705.1830 [hep-ph]. Cited in Section 6.1 (pg.152).
11. G. G. Raffelt and A. Y. Smirnov, "Adiabaticity and spectral splits in collective neutrino transformations," *Phys.Rev.* **D76** (2007) 125008, arXiv:0709.4641 [hep-ph]. Cited in Section 6.1 (pg.152).
12. A. Esteban-Pretel, A. Mirizzi, S. Pastor, R. Tomas, G. Raffelt, *et al.*, "Role of dense matter in collective supernova neutrino transformations," *Phys.Rev.* **D78** (2008) 085012, arXiv:0807.0659 [astro-ph]. Cited in Section 6.1 (pg.152).

13. H. Duan and J. P. Kneller, "Neutrino flavour transformation in supernovae," *J.Phys.G* **G36** (2009) 113201, arXiv:0904.0974 [astro-ph.HE]. Cited in Section 6.1 (pg.152).
14. B. Dasgupta, A. Dighe, G. G. Raffelt, and A. Y. Smirnov, "Multiple Spectral Splits of Supernova Neutrinos," *Phys.Rev.Lett.* **103** (2009) 051105, arXiv:0904.3542 [hep-ph]. Cited in Section 6.1 (pg.152).
15. H. Duan, G. M. Fuller, and Y.-Z. Qian, "Collective Neutrino Oscillations," *Ann.Rev.Nucl.Part.Sci.* **60** (2010) 569–594, arXiv:1001.2799 [hep-ph]. Cited in Section 6.1 (pg.152).
16. H. Duan and A. Friedland, "Self-induced suppression of collective neutrino oscillations in a supernova," *Phys.Rev.Lett.* **106** (2011) 091101, arXiv:1006.2359 [hep-ph]. Cited in Sections 6.1 (pg.152) and 6.2 (pg.155).
17. J. F. Cherry, J. Carlson, A. Friedland, G. M. Fuller, and A. Vlasenko, "Halo Modification of a Supernova Neutronization Neutrino Burst," *Phys.Rev.* **D87** (2013) 085037, arXiv:1302.1159 [astro-ph.HE]. Cited in Section 6.1 (pg.153).
18. J. F. Beacom, R. Boyd, and A. Mezzacappa, "Black hole formation in core collapse supernovae and time-of-flight measurements of the neutrino masses," *Phys.Rev.* **D63** (2001) 073011, arXiv:astro-ph/0010398 [astro-ph]. Cited in Section 6.1 (pg.153).
19. T. Fischer, S. C. Whitehouse, A. Mezzacappa, F. K. Thielemann, and M. Liebendorfer, "The neutrino signal from protoneutron star accretion and black hole formation," arXiv:0809.5129 [astro-ph], 2008. Cited in Section 6.1 (pg.153).
20. R. C. Schirato and G. M. Fuller, "Connection between supernova shocks, flavor transformation, and the neutrino signal," LA-UR-02-3068, arXiv:astro-ph/0205390 [astro-ph], 2002. Cited in Section 6.1 (pg.153).
21. F. Hanke, A. Marek, B. Muller, and H.-T. Janka, "Is Strong SASI Activity the Key to Successful Neutrino-Driven Supernova Explosions?," *Astrophys.J.* **755** (2012) 138, arXiv:1108.4355 [astro-ph.SR]. Cited in Section 6.1 (pg.153).
22. F. Hanke, B. Mueller, A. Wongwathanarat, A. Marek, and H.-T. Janka, "SASI Activity in Three-Dimensional Neutrino-Hydrodynamics Simulations of Supernova Cores," *Astrophys.J.* **770** (2013) 66, arXiv:1303.6269 [astro-ph.SR]. Cited in Section 6.1 (pg.153).
23. A. Friedland and A. Gruzinov, "Neutrino signatures of supernova turbulence," LA-UR-06-2202, arXiv:astro-ph/0607244 [astro-ph], 2006. Cited in Section 6.1 (pg.153).
24. T. Lund and J. P. Kneller, "Combining collective, MSW, and turbulence effects in supernova neutrino flavor evolution," arXiv:1304.6372 [astro-ph.HE], 2013. Cited in Section 6.1 (pg.153).
25. G. G. Raffelt, "Particle Physics from Stars," *Ann. Rev. Nucl. Part. Sci.* **49** (1999) 163–216, arXiv:hep-ph/9903472. Cited in Section 6.1 (pg.153).
26. P. Antonioli *et al.*, "Snews: The supernova early warning system," *New J. Phys.* **6** (2004) 114, astro-ph/0406214. Cited in Section 6.1 (pg.153).

27. K. Scholberg, "The SuperNova Early Warning System," *Astron. Nachr.* **329** (2008) 337–339, arXiv:0803.0531 [astro-ph]. Cited in Section 6.1 (pg.153).
28. A. Bueno, I. Gil Botella, and A. Rubbia, "Supernova neutrino detection in a liquid argon TPC," ICARUS-TM-03-02, arXiv:hep-ph/0307222 [hep-ph], 2003. Cited in Section 6.1 (pg.153).
29. S. Amoruso *et al.*, **ICARUS Collaboration** , "Measurement of the mu decay spectrum with the ICARUS liquid argon TPC," *Eur.Phys.J.* **C33** (2004) 233–241, arXiv:hep-ex/0311040 [hep-ex]. Cited in Section 6.2 (pg.154).
30. K. Scholberg *et al.*, "SNOwGLoBES: SuperNova Observatories with GLoBES." http://www.phy.duke.edu/~schol/snowglobes. Cited in Section 6.2 (pg.154).
31. S. Agostinelli *et al.*, **GEANT4** , "GEANT4: A simulation toolkit," *Nucl. Instrum. Meth.* **A506** (2003) 250–303. Cited in Section 6.2 (pg.154).
32. E. D. Church, "LArSoft: A Software Package for Liquid Argon Time Projection Drift Chambers," arXiv:1311.6774 [physics.ins-det], 2013. Cited in Section 6.2 (pg.154).
33. T. Totani, K. Sato, H. E. Dalhed, and J. R. Wilson, "Future detection of supernova neutrino burst and explosion mechanism," *Astrophys. J.* **496** (1998) 216–225, arXiv:astro-ph/9710203. Cited in Section 6.2 (pg.155).
34. J. Gava, J. Kneller, C. Volpe, and G. C. McLaughlin, "A dynamical collective calculation of supernova neutrino signals," *Phys. Rev. Lett.* **103** (2009) 071101, arXiv:0902.0317 [hep-ph]. Cited in Section 6.2 (pg.155).
35. L. Hudepohl, B. Muller, H.-T. Janka, A. Marek, and G. Raffelt, "Neutrino Signal of Electron-Capture Supernovae from Core Collapse to Cooling," *Phys.Rev.Lett.* **104** (2010) 251101, arXiv:0912.0260 [astro-ph.SR]. Cited in Section 6.2 (pg.155).
36. A. Cherry, A. Friedland, and H. Duan, "Private communication.".
37. M. T. Keil, G. G. Raffelt, and H.-T. Janka, "Monte Carlo study of supernova neutrino spectra formation," *Astrophys.J.* **590** (2003) 971–991, arXiv:astro-ph/0208035 [astro-ph].
38. E. Church *et al.*, "Muon-induced background for beam neutrinos at the surface," LBNE-doc-6232, October, 2012. Cited in Section 6.3.1 (pg.158).
39. Gehman, V. and Kadel, R, "Calculation of intrinsic and cosmogenic backgrounds in the LBNE far detector for use in detection of supernova neutrinos," LBNE-doc-8419, January, 2014. Cited in Section 6.3.2 (pg.159).
40. J. H. Harley *et al.*, "Report No. 094 - Exposure of the Population in the United States and Canada from Natural Background Radiation," *National Council on Radiation Protection and Measurements* (2014) . http://www.ncrppublications.org/Reports/094. Cited in Section 6.3.3 (pg.160).
41. L. Grandi, "Darkside-50: performance and results from the first atmospheric argon run," February, 2014. UCLA's 11th Symposium on Sources and Detection of Dark Matter and Dark Energy in the Universe. Cited in Section 6.3.3 (pg.160).
42. D. Leonard, P. Grinberg, P. Weber, E. Baussan, Z. Djurcic, *et al.*, "Systematic study of trace radioactive impurities in candidate construction materials for EXO-200,"

Nucl.Instrum.Meth. **A591** (2008) 490–509, arXiv:0709.4524 [physics.ins-det]. Cited in Section 6.3.3 (pg.160).